Modern organophotocatalysts: a new inspiration source for Symmetrical Organic Redox Flow Batteries

Jules Moutet, Mubarak Md Hossain, Ramandeep Kaur, Tarek H. El-Assaad, Waleed K. Yual, Janelle M. Amegatse and Thomas L. Gianetti*

University of Arizona, Department of Chemistry and Biochemistry, Tucson, AZ, 85750 United States

*E-mail: tgianetti@arizona.edu

TOC

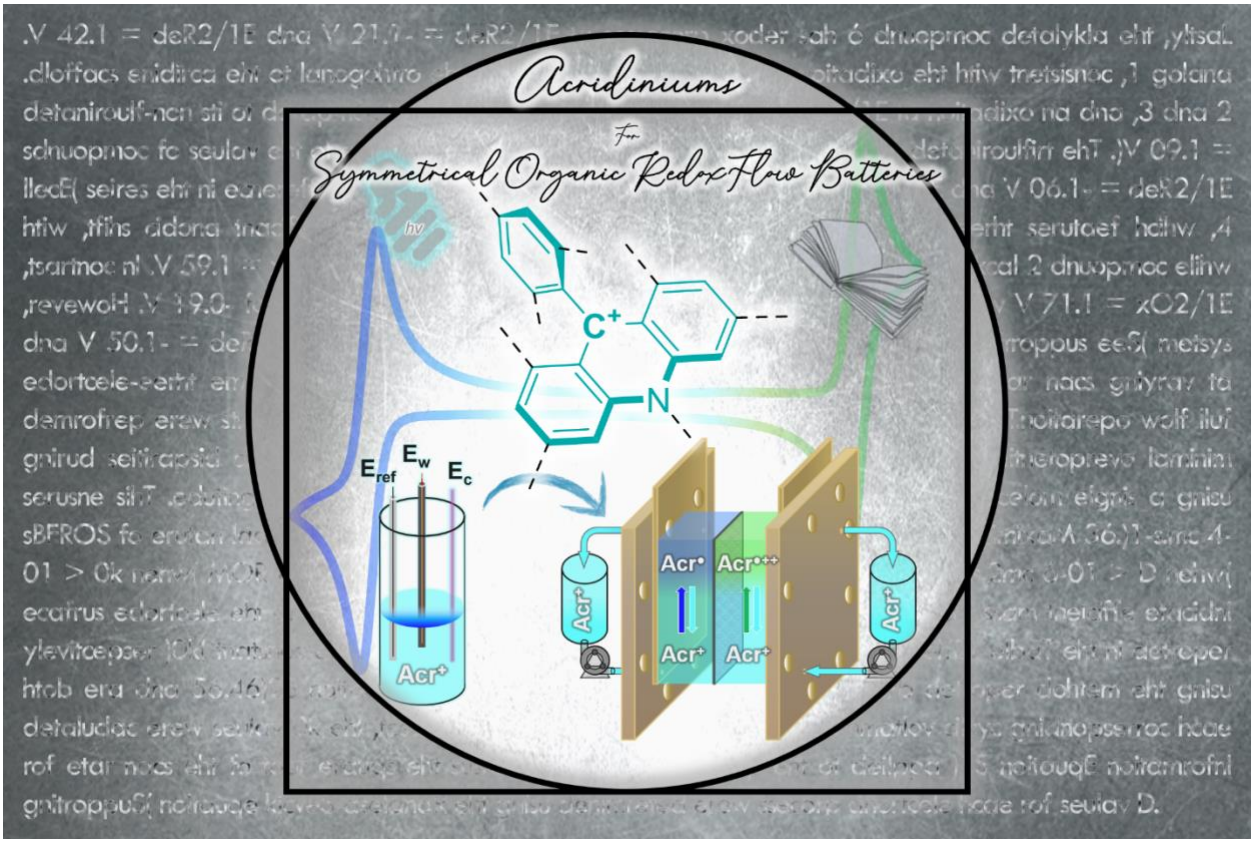

KEY-WORDS

Symmetrical Organic Redox flow battery – organophotocatalyst – acridinium – energy - electrochemistry

ABSTRACT

Redox flow batteries (RFBs) have emerged as significant energy storage systems amid the growing adoption of renewable energy. However, the advancement of all-organic RFBs is hindered by

material crossover, limited energy density, and the time-consuming selection of suitable electrolyte partners. To address these challenges, bipolar redox-active organic molecules (BRMs) show promise for charge storage in symmetric organic redox flow batteries (SORFBs), although their development can be complex and tedious. In this study, we report an approach aimed at streamlining the identification of suitable compounds through an examination of the organophotocatalyst literature, illustrated through six acridinium compounds exhibiting stable redox states. These compounds were thoroughly characterized in electrochemical cells and subjected to cycling tests in fully symmetric flow batteries. Notably, a trisubstituted electron-rich acridinium compound emerged as a potential candidate, demonstrating over 20 days of cycling stability. Given the extensive library of organic catalysts and the advantages of SORFB designs, this approach will prove to be essential for developing an innovative electrochemical storage system.

INTRODUCTION

The intermittent nature of renewable energies presents a significant challenge to their widespread adoption, necessitating the development of advanced energy storage solutions for grid integration, which are decisive for decarbonizing the economy and facing climate change.[1–3] Within the field of electrochemical storage, lithium-ion batteries[4–6] and other metal-based solutions[7–10] have been successfully implemented. However, safety concerns related to fire hazards from low valent metal accumulation and the dwindling availability of these materials[11,12] is inciting the industry to seek safer, cost-effective, and scalable electricity energy storage (EES) solutions.[13–15] Redox Flow Batteries (RFBs) have since gained attention for large-scale stationary applications due to their engineering flexibility and scalability, enabled by the decoupling of power and capacity.[16–19] Although, first developed in the 1930s, revisited in 1970s within NASA's space program and based on metals-ions in acid,[20] RFBs are recently experiencing renewed interest with the introduction of non-aqueous approach.[21–23] This also enable the use of Redox-active Organic Molecules (ROMs), which offer improved sustainability compared to transition metal-based materials, with a significantly lower environmental impact, while offering greater tunability.[24,25] The use of two distinct ROMs as catholyte and anolyte, which unfortunately can leak into the opposite compartment, causing chemical degradation and irreversible capacity fading,[26,27] has been identified as a bottleneck in developing Asymmetric RFB EES. That's why, a promising solution, have gained prominence with the emergence of Symmetrical Organic Redox Flow Batteries (SORFBs) that's eliminating ROMs membrane crossover and prolonging EES lifespan.[28–31] The key feature of SORFBs is their use of a single bipolar redox molecule (BRM) on both sides of the cell.[32,33] Those robust molecules possess at least three stable redox states thanks to fully reversible reduction and oxidation processes, allowing them to act as both anolyte and catholyte depending of the polarity.[34–36] An SORFB employs identical solution components in each half-cell, providing distinct advantages:[28] Using the same redox-active material decreases the chemical gradient of electroactive species, eliminating the need for highly selective membranes and effectively minimizing crossover. In cases of leak, instead of permanent contamination, the SORFBs

experience self-discharge.[30] When in a discharged state, the absence of a chemical gradient across the membrane ensures that SORFBs can be stored indefinitely without contamination from leakage or irreversible side reactions. Recent studies have also shown that capacity loss due to compound degradation can be recovered through regular polarity reversals, thereby extending the battery's lifespan.[28,37–39] Furthermore, relying on a unique charge carrier molecule can lead to substantial saving when scaling-up while rationalizing the supply chain for commercialization.[40]

Recent advancements in SORFB research have inspired the design of various BRMs through different strategies:[41] a "combi-molecule" approach,[42,43] using insulating links or merging defined scaffolds, and on the other hand a focus on molecules with three inherent stable redox states. In latter approach, our research group has highlighted the use of dimethoxyquinacridinium[44–46] and triangulenium[47] BRMs as charge carriers in SORFBs. Notably, we have also demonstrated that these classes of carbocations can function as bimodal organic photocatalysts,[48–50] catalyzing both oxidation and reduction reactions depending on the present electron donors or acceptors, thanks to their three stable redox states. This leads us to propose a method for identifying new relevant BRMs for SORFB deployment by exploring bimodal photocatalysts from the literature.[51] Given its prominence in modern photocatalysis and our contribution to its bimodal use,[52,53] we have chosen the acridinium family— a stable carbocation recognized for its robust and tunable synthesis[54]—as a benchmark core molecule. This work will demonstrate how accessible or commercially available bimodal photoredox catalysts can lead to relevant BRMs for symmetrical flow batteries. This principle will be exemplified by evaluating six different acridinium compounds, leveraging our expertise in SORFB deployment. The study will involve electrochemical characterization using a three-electrode cell to investigate the impact of scaffold variations on electrochemical kinetics parameters and their suitability as ROMs. Finally, we will assess the durability of the BRMs, which have shown promising properties for redox flow battery applications, through cycling tests in a complete SORFB prototype.

RESULTS AND DISCUSSION

The choice of the acridinium class of compounds for this study is based on their widespread use as organophotocatalysts, their synthetic versatility, and their commercial availability. Their application as bipolar redox materials in symmetric organic redox flow batteries (SORFBs) lies on their ability to exhibit -for some of them- three stable oxidation states, specifically the reversible reduction of $\mathbf{Acr^+ \leftrightharpoons Acr^\bullet}$ and the reversible oxidation of $\mathbf{Acr^+ \leftrightharpoons Acr^{+\bullet}}$ (Figure 1).

In this work, we focus on compounds with a shared dihydroacridinium core and studied their ability to act as bipolar redox material for redox flow battery electrolytes. We studied the properties of six reference molecules (**1-6**). Compound **1,** 2,6-dimethoxyphenyl-1,8-dimethoxy-10-propylacridinium tetrafluoroborate, was first reported by Laursen *et. al* and is a precursor for the synthesis of quinacridium and triangulenium used in our group,[55] while its application as photocatalyst was by Lacour and co-workers.[56,57] 9-Mesityl-10-methylacridinium salt (**2**)[58] was introduced by Fukuzumi[59,60] and this along with numerous acridinium derivatives like 9-Mesityl-

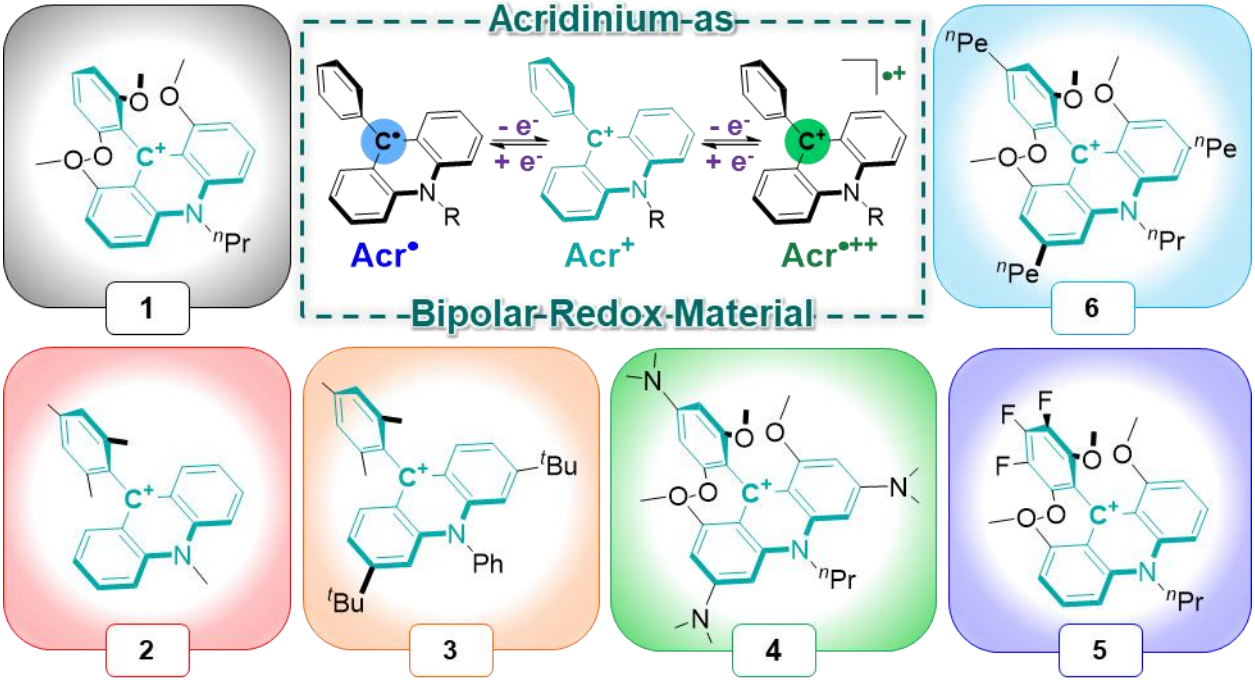

*Figure 1: Library of organophotocatalyst of the acridinium class explored in this work with **1**: 9-(2,6-diMeOPh)-1,8-diMeO-10-propyl-9,10-dihydroacridinium; **2**: 9-mesityl-10-methyl-9,10-dihydroacridinium; **3**: 3,6-di-tert-butyl-9-mesityl-10-phenyl-9,10-dihydroacridinium; **4**: 3,6-bis(dimethylamino)-9-(4-(dimethylamino)-2,6-diMeOphenyl)-1,8-diMeO-10-propyl-9,10-dihydroacridinium; **5**: 1,8-diMeO-10-propyl-9-(3,4,5-trifluoro-2,6-diMeOphenyl)-9,10-dihydroacridinium; **6**: 9-(2,6-diMeO-4-pentylphenyl)-1,8-diMeO-3,6-dipentyl-10-propyl-9,10-dihydroacridinium.*

3,6-di-tert-butyl-10-phenylacridinium salt (**3**),[61] were popularized as organophotocatalysts by the Nicewicz group.[54,62] Additionally, we investigated the properties of 3,6-bis(dimethylamino)-9-(4-(dimethylamino)-2,6-dimethoxyphenyl)-1,8-dimethoxy-10-propyl-9,10-dihydroacridinium tetrafluoroborate (**4**), which was developed by our group and used as a bimodal photocatalyst for alpha arylation of cyclic ketones.[53] Lastly, we examine 1,8-dimethoxy-10-propyl-9-(3,4,5-trifluoro-2,6-dimethoxyphenyl)-9,10-dihydroacridinium (**5**) and 9-(2,6-dimethoxy-4-pentylphenyl)-1,8-dimethoxy-3,6-dipentyl-10-propyl-9,10-dihydroacridinium (**6**), both recently synthesized within our research team. Compound **5**, through the introduction of three fluorine atoms on one of the aromatic rings, was designed to increase the Lewis acidity of the acridinium, thereby contributing to the stabilization of the **Acr$^{+\bullet}$** oxidation state (the synthesis of this novel compound is provided in the supporting information). On the other hand, compound **6** was developed (synthesis available in the supporting information) to induce an electron-donating effect

while also enhancing the potential solubility of the species by introduction of alkyl chain. The accessibility and stability of the three redox states **Acr•** ⇋ **Acr^{+}** ⇋ **Acr$^{++•}$** depicted in Figure 1 are essential for developing a suitable BRM for symmetrical RFBs, as these acridiniums will function as both the anolyte and catholyte. Therefore, the six molecules presented in this study must be compatible with the various oxidation states.

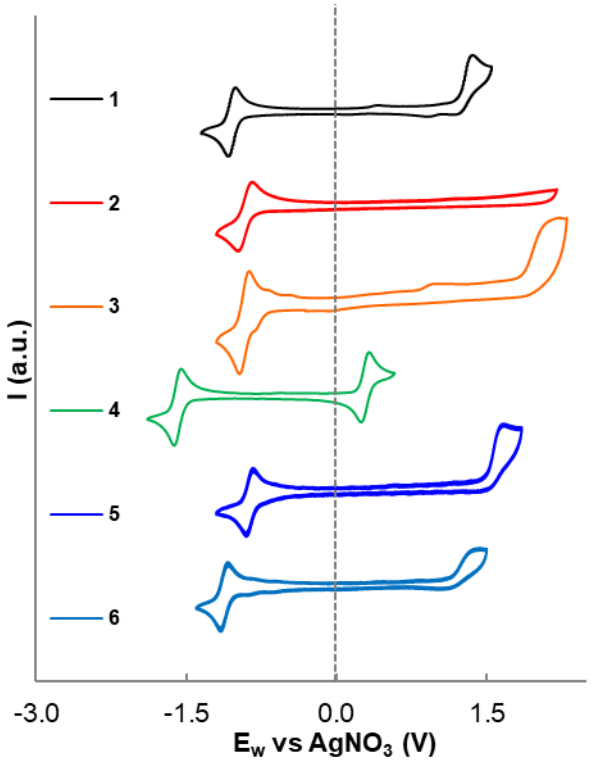

Figure 2: Cyclic voltammograms of 1 mM 1 to 6 in 0.1 M $TBAPF_6$ CH_3CN solution at 100 $mV{\cdot}s^{-1}$. All values of potential are reported in Table 1

Initially, we examined the electrochemical properties of these different compounds in acetonitrile, chosen as the optimal solvent for our investigation due to its wide electrochemical window (~6.0 V) and because it has been proven to be an ideal medium for acridinium based organophotocatalysis. Accordingly, we recorded the cyclic voltammograms (CVs) of these species at a concentration of 1 mM in a 0.1 M $TBAPF_6$ acetonitrile solution, using a scan rate of 100 $mV{\cdot}s^{-1}$. Each CV is depicted in the Figure 2, with the redox potentials for reversible monoelectronic reduction ($E_{1/2}^{Red}$) and oxidation ($E_{1/2}^{Ox}$) processes listed in Table 1.

Compound **1** displays two distinct events at $E_{1/2}^{Red}$ = -1.05 V and $E_{1/2}^{Ox}$ = 1.17 V vs $AgNO_3$. Acridinium **2** and **3** share the same $E_{1/2}^{Red}$ value of -0.91 V. However, while compound **2** lacks a reversible oxidation process, compound **3** exhibits $E_{1/2}^{Ox}$ = 1.95 V. In contrast, **4**, which features three electron-donating dimethylamine groups, shows a significant anodic shift, with $E_{1/2}^{Red}$ = -1.60 V and $E_{1/2}^{Ox}$ = -0.30 V, presenting the smallest potential difference in the series (E_{cell} = 1.90 V). The trifluorinated molecule **5**, displays a $E_{1/2}^{Red}$ = -0.87 V, close to the values of compounds **2** and **3**, and an oxidation at $E_{1/2}^{Ox}$ = -1.54 V, a 400mV cathodic shift compared to its non-fluorinated analog **1,** consistent with the oxidation occurring on the phenyl ring the orthogonal to the acridine scaffold. Lastly, the alkylated compound **6** has redox processes at $E_{1/2}^{Red}$ = -1.12 V and $E_{1/2}^{Red}$ = 1.24 V.

To assess the reversibility of these redox processes, CV measurements were performed at varying scan rates of 10, 25, 75, 100, 250, 400, and 500 $mV.s^{-1}$ in the same three-electrode system (See supporting information).

The diffusion coefficient (D) and the electron transfer rate constant (k^0) respectively indicate efficient mass transport of the redox-active species from the bulk solution to the electrode surface (when D > 10^{-6} $cm^2.s^{-1}$) and effective electron transfer from the electrodes to the ROM (when k^0 >

10^{-4} cm.s^{-1}).[63] Maximizing D and k^0 is crucial in the context of BRMs and the symmetrical nature of SORFBs using a single molecule to keep the reduction and oxidation values at a similar magnitude. This ensures minimal overpotential and maximizes energy efficiency by avoiding significant kinetic disparities during full flow operation.

D values for each electronic process were determined using the Randles–Sevcik equation (Supporting Information Equation S1) applied to the plot of peak current versus the square root of the scan rate for each corresponding cyclic voltammogram (CV). Based on the same dataset, the k^0 values were calculated using the method reported by Lavagnini *et al.* (Supporting Information Equation S2)[64,65] and are both reported in the Table 1.

Table 1: Summary of $E_{1/2}^{Red/Ox}$, E_{gap}, diffusion parameters (D) and electron-transfer rate parameters (k^0) of each Acr^+ measured at 1 mM in 0.1 M $TBAPF_6$ CH_3CN. Potentials are expressed against $AgNO_3/Ag$.

Acridinium	$E_{1/2}^{Red}$ (V)	$E_{1/2}^{Ox}$ (V)	E_{Cell} (V)	D (× 10^{-6} cm²/s) †		k^0 (× 10^{-2} cm/s) ‡	
				$E_{1/2}^{Red}$	$E_{1/2}^{Ox}$	$E_{1/2}^{Red}$	$E_{1/2}^{Ox}$
1	-1.05	1.17	2.22	7.85	6.70	2.07	0.03
2	-0.91	-	-	11.7	-	1.00	-
3	-0.92	1.95	2.87	9.47	1.41	0.59	0.03
4	-1.60	0.30	1.90	10.3	7.87	2.59	1.09
5	-0.87	1.54	2.41	11.1	16.4	18.1	0.09
6	-1.12	1.24	2.36	7.70	4.66	1.45	0.04

† Obtained by application of the Randles–Sevcik equation.
‡Obtained thanks to the numerical approach developed by Lavagnini *et al.*

The acridinium **1** exhibits diffusion coefficients, D_{Red} and D_{Ox}, of 7.9 and 6.7 × 10^{-6} cm^2.s^{-1}, respectively. While the electron transfer rate in the reduction process is efficient (k^0_{Red} = 2.1 × 10^{-2} cm.s^{-1}), the k^0_{Ox} is significantly lower by two orders of magnitude, with a value of 0.03 × 10^{-2} cm.s^{-1}, a strong difference that can be a source of issues in battery cycling. Compound **2** does not display any accessible reversible electrochemical process in oxidation, it is therefore disqualified as a candidate for a bipolar redox mediator (BRM) and will not be discussed further. However, it could meet potential use as a robust negolyte in asymmetric batteries, since its electrokinetic parameter D_{Red} and k^0_{Red} are fitting the requirement to be use in ORFB.

Compound **3** presents high diffusion parameters with similar magnitude for the oxidation and reduction events, with D_{Red} and D_{Ox} at 9.5 and 1.4 × 10^{-6} $cm^2.s^{-1}$, respectively. However, its electron transfer rates are low, with k^0_{Red} = 0.59 × 10^{-2} $cm.s^{-1}$ and k^0_{Ox} = 0.03× 10^{-2} $cm.s^{-1}$, and differ by more than an order of magnitude between the two events, raising concerns about potential negative effects on electron transport under cycling condition. Compound **4**, in contrast, appears particularly promising, exhibiting high diffusion coefficients (D_{Red} = 10.3 × 10^{-6} $cm^2.s^{-1}$ and D_{Ox} = 1.4 × 10^{-6} $cm^2.s^{-1}$) and electron transfer rates of the same order of magnitude, k^0_{Red} and k^0_{Ox} with values of 2.6 and 1.1× 10^{-2} $cm.s^{-1}$ respectively. Compound **5**, meanwhile, offers very high diffusion coefficients, exceeding 11.1 × 10^{-6} $cm^2.s^{-1}$, highlighting the beneficial impact of fluorine atoms on diffusion in organic solvents. However, a problematic kinetic discrepancy is observed, with k^0_{Red} = 18.1 × 10^{-2} $cm.s^{-1}$ and k^0_{Ox} = 0.09 × 10^{-2} $cm.s^{-1}$, a three-order-of-magnitude difference, signaling issues with the oxidation process. Lastly, compound **6**, the alkylated derivative of **1**, exhibits diffusion parameters close to each other's and in the range of those of compound **4**, with D_{Red} = 7.7 × 10^{-6} $cm^2.s^{-1}$ and D_{Ox} = 4.7 × 10^{-6} $cm^2.s^{-1}$. However, similar to **1**, **3** and **5**, electron transfer rates difference, by two orders of magnitude (k^0_{Red} = 1.45 × 10^{-2} $cm.s^{-1}$ and k^0_{Ox} = 0.04 × 10^{-2} $cm.s^{-1}$) suggests future electrochemical problems under battery testing conditions.

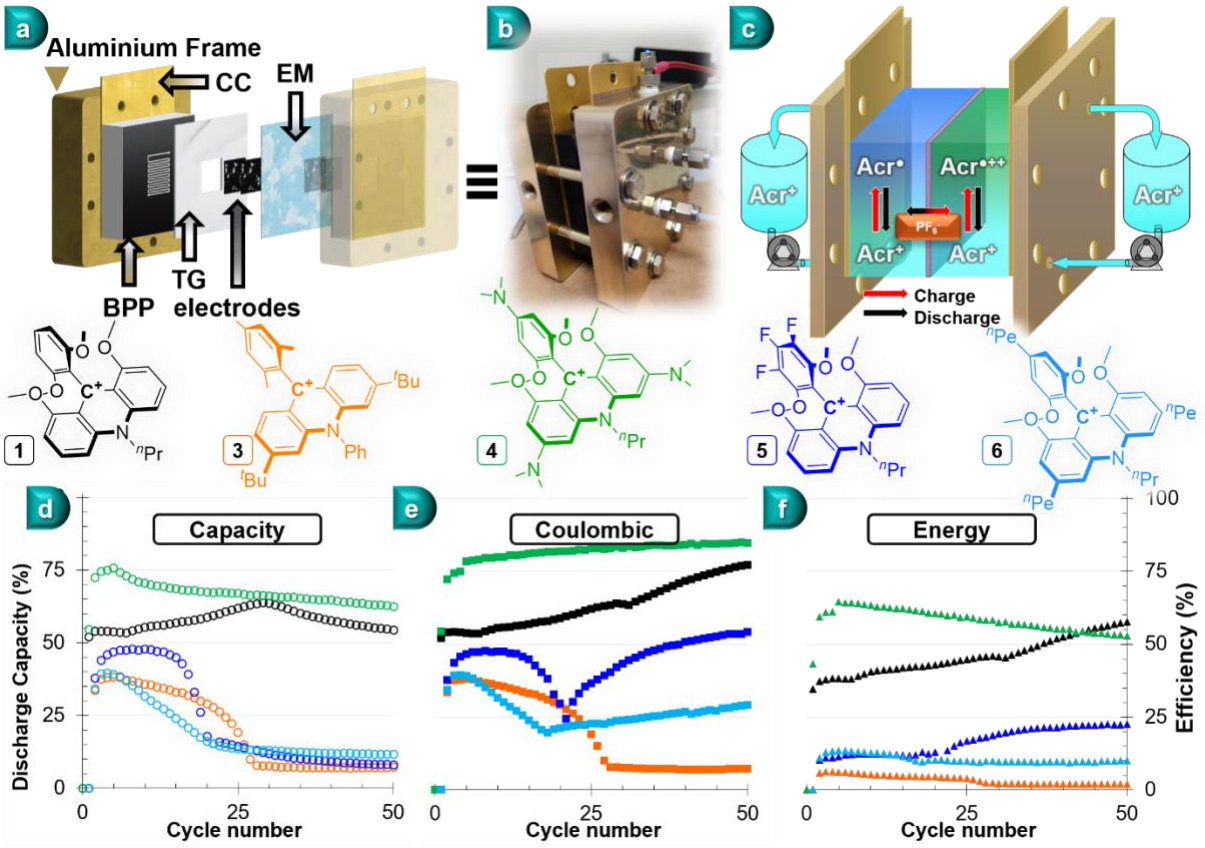

Figure 3: a) Scheme of assembly of the RFB cell prototype. b) Picture of the assembled cell. c) Scheme of the SORFB cell during cycling of acridinium d) Discharge capacity (circles), e) Coulombic Efficiency (squares) and f) Energy Efficiency (triangles) vs cycle number for RFB-cell cycling with tanks loaded each with 4mL of 1 mM ***Acr***$^+$ *in 0.1M TBAPF₆ CH₃CN, flow 16mL/min per channel, 2 C-rate for 50 cycles ~50h. Each data point represents one cycle.*

These results provide a detailed analysis of the properties of these different compounds, but to evaluate their potential as BRMs under practical conditions, we decided to conducted complete redox flow cell studies. For this purpose, we relied on a fully symmetric organic redox flow battery (SORFB) prototype (Figure 3 a, b, c). The flow cell was equipped with bipolar graphite plates (BPP) featuring a serpentine flow pattern and carbon-felt electrodes. These electrodes have 80% porosity and an electrical resistivity of less than 5 mΩ.cm². Surface chemistry analysis of the electrodes, as reported in the literature, confirmed their suitability for the development of non-aqueous organic redox flow batteries (NAqORFB).[66] The cell compartments were separated by a Daramic-175 porous membrane, serving as an ion-exchange separator for counter anions (EM). Teflon gaskets (TG) were used in the flow cell to avoid leakage of liquid. During galvanostatic cycling, electrolyte solutions flowed through the cell at a rate of 16 mL/min. Charging and discharging were performed at a constant current, corresponding to a 2C rate, until a voltage cutoff of +200 mV from the cell's theoretical E_{cell} (as detailed in the Table 1) was reached, with a 100% state of charge (SOC) limit applied. The discharge cutoff was set at 0 V, corresponding to 0% SOC. At the interface, charges generated on the BRM were compensated by the migration of PF_6^- counter anions through the permeable exchange membrane (Figure 3 c).

To efficiently evaluate performance, we limited the number of charge-discharge cycles per compound to 50, allowing us to assess the behavior of these different BRMs over a 2-day period. For compound **1** (black plot Figure 3 d, e, f), the initial discharge capacity was 54%, which slightly increased before a slight decreased stabilizing at 51% by cycle 50. Notably, the coulombic efficiency improved from 54% to 78% between the first and last cycles, suggesting that this acridinium undergoes transformations over time, becoming more effective. However, post-cycling NMR analyses of the solutions could not clarify the underlying chemical mechanisms. Compound **2** was excluded from the tested BRMs as it was not viable and will not be discussed further.

Compound **3** (orange plot) encountered significant difficulties from the first cycles, with discharge capacities below 35%, rapidly declining to less than 8% by cycle 28. A similar trend was observed for the coulombic efficiency, which corresponded to poor energy efficiency, starting at 6% and dropping to 2% by cycle 28, rendering this compound a poor BRM candidate.

Acridinium **4** (green plot), as expected based on the electrokinetic parameters measured in Table 1, exhibited promising results, with an initial discharge capacity of 75%, which gradually decreased to 62% by cycle 28. Similar to compound **1**, compound **4** showed an increase in coulombic efficiency throughout the experiment, reaching a peak value of 85% after 50 cycles. This also resulted in decent energy efficiency, which declined from 65% to 53% over the course of the 50 cycles.

As anticipated due to its electron transfer rate discrepancies, the trifluorinated compound **5** underperformed (dark blue plot), with a discharge capacity of 46% during the first 15 cycles, followed by a sudden drop to 15% at cycle 22, eventually reaching 8% by cycle 50. The coulombic efficiency exhibited unusual behavior, with a drop analogous to the discharge capacity at cycle 18,

followed by a rebound, though this was not significant and further studied given the low energy storage (EE below 25%).

Finally, the alkylated compound **6** (light blue plot) showed a decrease in discharge capacity from 39% to 11%, alongside a low energy efficiency, averaging around 11%, with a not significant coulombic efficiency, again result expect due to the discrepancy of kinetic rates between the two redox events.

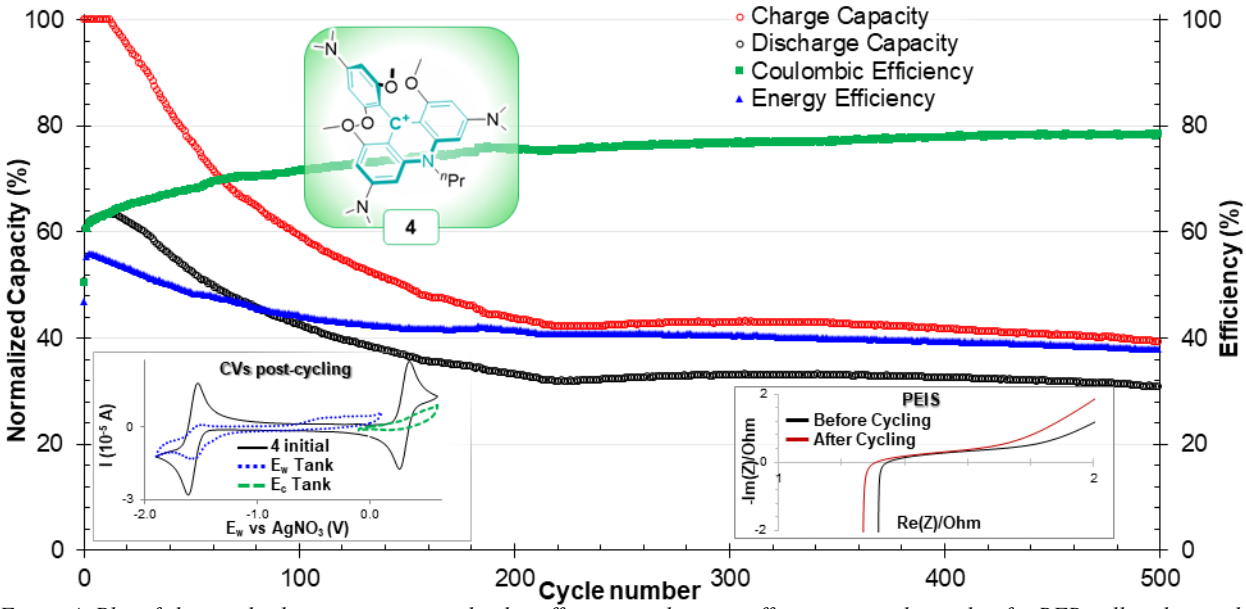

*Figure 4: Plot of charge, discharge capacity, coulombic efficiency and energy efficiency vs cycle number for RFB-cell cycling with tankers loaded each with 4mL of 1 mM **4**, flow 16mL/min per channel, 2 C-rate for 500 cycles ~21 days. Each data point represents one cycle. Left insert: CVs of tank's solutions after 500 cycles and comparison with initial **4** CV. Right insert: PEIS of the cell in flow before and after 500 cycles (both at 0% SOC) from 1Ghz to 0.1Hz with an amplitude of 10mV.*

Clearly, acridinium **4** stands out significantly compared to the other compounds presented in this study. We therefore repeated the full SORFB experiment with this compound over a longer period of time. We allowed the battery to cycle for 500 cycles, approximately 21 days. The data collected revealed two distinct operational regimes for this compound. In the first dozen cycles, the battery reached its full charge capacity, but the maximum discharge capacity only reached 65%. Subsequently, both charge and discharge capacities began to decline at rates of 0.28% and 0.16% per cycle, respectively, until stabilizing at around cycle 220. At this point, both capacities leveled off, decreasing by only 0.05% per cycle, ultimately resulting in a charge capacity of 39% and a discharge capacity of 31%. The Coulombic efficiency mirrored this stabilization, initially improving over the first 220 cycles from 61% to 75%, then gradually reaching 79% by cycle 500. Interestingly, the variations in energy efficiency were less pronounced, starting at a relatively high 55% in the early cycles and dropping to 41% by cycle 220, before stabilizing at an average of 40% for the remainder of the experiment.

To rationalize the important capacity loss over the first 200 cycles, we performed cyclic voltammetry (CV) analysis of the content in each battery tank after 500 cycles (Figure 4 left insert).

We observed that the reduction process (E_w) tank lost 29% of its peak area during the experiment, whereas the oxidation process in the E_c tank saw a more significant loss of 54%. This underscores the excellent performance of acridiniums as negolytes in ORFBs, but also highlights that their oxidation processes need improvement to enhance overall properties.

Recent techno-economic analyses have established an area-specific resistance (ASR) target of under 5 Ω/cm² to optimize NAqORFB design.[67] To assess the scalability of our prototype, we conducted potential electrochemical impedance spectroscopy (PEIS) at 0% SOC (when the SORFB is at equilibrium, $\mathbf{Acr^+}$/$\mathbf{Acr^+}$) before and after cycling (Figure 4 right insert). It was found that after 500 cycles, the interface resistivity between the two sides of the battery slightly decreased, from 1.35 Ω to 1.31 Ω. Although minor, this consistent difference observed in experiments with acridinium **4** suggests that some of the missing redox-active material in the battery tanks may have deposited onto the electrodes/EM, forming a layer that contributed to partial charge storage. This finding, unexpectedly mentioned in another of our studies,[47] leads us to believe that further investigation is needed on the electrode materials and their role in the stability of BRM compounds.

CONCLUSION

In this work, we introduced a novel approach for developing SORFBs by focusing on existing molecules with three stable redox states suitable as BRMs. The rapid advancements in organic photocatalysis proved valuable, as many bimodal catalysts from this field meet the criteria for multiple stable oxidation states. We emphasized on the importance of detailed electrochemical and electrokinetic analyses (D and k^0 parameters) of these redox-active molecules to assess their potential as charge carrier in flow batteries, demonstrating how subtle structural variations can significantly affect their robustness and suitability. Out of the six acridinium-based model compounds tested, five showed promises in our RFB prototype, with compound **4**, developed by our group, achieving over 20 hours of cycling in a SORFB. This work highlights the strong synergy that can exist between organic catalysis and its growing library of compounds, and the identification of unsuspected ROMs for the deployment of symmetrical organic batteries. We hope that this approach will inspire further research and accelerate progress in the development of innovative SORFB.

EXPERIMENTAL

General remarks

All solvents were purified using SPS or by distillation over the specified drying agents. Dried solvents and liquid reagents were transferred via syringes pre-dried in an oven. The supporting electrolyte, tetrabutylammonium hexafluorophosphate ($TBAPF_6$), was recrystallized three times from ethanol and dried at 80°C for three days before use inside the glovebox. All glassware and equipment were oven-dried for at least 24 hours prior to glovebox introduction.

9-Mesityl-10-methylacridinium tetrafluoroborate (**2**) and 9-Mesityl-3,6-di-tert-butyl-10-phenylacridinium tetrafluoroborate (**3**) were purchased from Sigma Aldrich, dried under vaccuum overnight and then introduced into the Argon glovebox. Synthesis details for new acridinium compounds are provided in the Supplementary Materials.

Electrochemical studies

Electrochemical measurements were performed inside an argon-filled MBraun Unilab glovebox, utilizing a BioLogic SP-200 potentiostat/galvanostat and EC-Lab software (v11.50). For convenience, potentials were referenced to either an internal $AgNO_3$/Ag electrode or to the cell itself in a two-electrode configuration. Cyclic voltammograms (CVs) were obtained in a three-electrode electrochemical cell comprising a platinum wire counter electrode, an $AgNO_3$/Ag reference electrode (0.01 M $AgNO_3$ in 0.1 M $TBAPF_6$ in CH_3CN), and a glassy carbon working electrode (0.071 cm², CH Instruments, Inc.). Prior to each measurement, the working electrode was polished using aluminum oxide on polishing paper and rinsed with anhydrous CH3CN to eliminate residual particles. Diffusion coefficient (D) and electron transfer rate constant (k^0) values were determined from CVs recorded at various scan rates (10, 25, 75, 100, 250, 400, and 500 $mV.s^{-1}$) in a CH_3CN electrolyte solution containing 1 mM Acr^+ and 0.1 M $TBAPF_6$.

Redox flow battery experiments

Flow cell experiments were carried out using a BioLogic SP-200 in galvanostatic mode, operated through EC-Labs software (v11.50), within an argon-filled glovebox. A 5 cm² single-cell flow battery was employed, with a PTFE gasket on each side featuring a 5 cm² cutout for the exchange surface, accommodating two carbon felt electrodes that were in direct contact with the central exchange membrane. This membrane consisted of porous separators positioned between the anolyte and catholyte compartments (Figure 3 a). The flow cell components were oven-dried overnight, assembled outside the glovebox, and promptly transferred into the glovebox via the antechamber. Both anolyte and catholyte reservoirs were filled with 4 mL of electrolyte/ROM in 0.1 M $TBAPF_6$ in CH_3CN at 1mM concentration. The electrolyte was circulated through the flow cell using a peristaltic pump at a flow rate of 16 mL $min.s^{-1}$. A 4-hour equilibration period preceded active charging and discharging. Details and dimensions are available in Supplementary Materials.

Authors' contributions

The manuscript was prepared with contributions from all authors, who approved the final version. J.M. and T.L.G. authored the manuscript and discussed the conclusions. J.M. designed the experiments and performed all electrochemical studies; M.H. developed and synthesized compound **4**; T.H.E. developed, synthesized, and characterized compound **5**; R.K. developed and synthesized compound **6**; W.Y. and J.A. replicated the electrochemical cycling experiments.

Acknowledgements & Funding Sources

Financial support comes from the University of Arizona, and Research Corporation for Science Advancement Cottrell Scholarship 2021 (Award #27536). All NMR data were collected in the NMR facility of the Department of Chemistry and Biochemistry at the University of Arizona, RRID:SCR_012716. The purchase of the Bruker NEO 500 MHz spectrometer was supported by the National Science Foundation under Grant Number 1920234 and the University of Arizona. J.M. is grateful to Angelica P. Orlova for stimulating and inspiring discussions.

REFERENCES

(1) Dresselhaus, M. S.; Thomas, I. L. Alternative Energy Technologies. *Nature* **2001**, *414* (6861), 332–337.

(2) Weitemeyer, S.; Kleinhans, D.; Vogt, T.; Agert, C. Integration of Renewable Energy Sources in Future Power Systems: The Role of Storage. *Renew. Energy* **2015**, *75*, 14–20.

(3) Gür, T. M. Review of Electrical Energy Storage Technologies, Materials and Systems: Challenges and Prospects for Large-Scale Grid Storage. *Energy Environ. Sci.* **2018**, *11* (10), 2696–2767.

(4) Goodenough, J. B.; Whittingham, M. S.; Yoshino, A. The Nobel Prize in Chemistry 2019 "for the Development of Lithium-Ion Batteries." *R. Swedish Acad. Sci.* **2019**, https://www.nobelprize.org/prizes/chemistry/2019/p.

(5) Masias, A.; Marcicki, J.; Paxton, W. A. Opportunities and Challenges of Lithium Ion Batteries in Automotive Applications. *ACS Energy Lett.* **2021**, 621–630.

(6) Wu, J.; Zhou, T.; Zhong, B.; Wang, Q.; Liu, W.; Zhou, H. Designing Anion-Derived Solid Electrolyte Interphase in a Siloxane-Based Electrolyte for Lithium-Metal Batteries. *ACS Appl. Mater. Interfaces* **2022**, *14* (24), 27873–27881.

(7) Hirsh, H. S.; Li, Y.; Tan, D. H. S.; Zhang, M.; Zhao, E.; Meng, Y. S. Sodium-Ion Batteries Paving the Way for Grid Energy Storage. *Adv. Energy Mater.* **2020**, *10* (32).

(8) Shang, W.; Yu, W.; Liu, Y.; Li, R.; Dai, Y.; Cheng, C.; Tan, P.; Ni, M. Rechargeable Alkaline Zinc Batteries: Progress and Challenges. *Energy Storage Mater.* **2020**, *31* (March), 44–57.

(9) Buckingham, R.; Asset, T.; Atanassov, P. Aluminum-Air Batteries: A Review of Alloys, Electrolytes and Design. *J. Power Sources* **2021**, *498* (March), 229762.

(10) Huang, H.; Li, D.; Hou, L.; Du, H.; Wei, H.; Liu, X.; Wang, Q.; Wei, Y. Advanced Protective Layer Design on the Surface of Mg-Based Metal and Application in Batteries: Challenges and Progress. *J. Power Sources* **2022**, *542* (June), 231755.

(11) Tarascon, J.-M.; Armand, M. Issues and Challenges Facing Rechargeable Lithium Batteries. *Nature* **2001**, *414* (6861), 359–367.

(12) Winter, M.; Barnett, B.; Xu, K. Before Li Ion Batteries. *Chem. Rev.* **2018**, *118* (23), 11433–11456.

(13) Yang, Z.; Zhang, J.; Kintner-Meyer, M. C. W.; Lu, X.; Choi, D.; Lemmon, J. P.; Liu, J. Electrochemical Energy Storage for Green Grid. *Chem. Rev.* **2011**, *111* (5), 3577–3613.

(14) Badwal, S. P. S.; Giddey, S. S.; Munnings, C.; Bhatt, A. I.; Hollenkamp, A. F. Emerging Electrochemical Energy Conversion and Storage Technologies. *Front. Chem.* **2014**, *2* (September), 1–28.

(15) Trahey, L.; Brushett, F. R.; Balsara, N. P.; Ceder, G.; Cheng, L.; Chiang, Y. M.; Hahn, N. T.; Ingram, B. J.; Minteer, S. D.; Moore, J. S.; Mueller, K. T.; Nazar, L. F.; Persson, K.

A.; Siegel, D. J.; Xu, K.; Zavadil, K. R.; Srinivasan, V.; Crabtree, G. W. Energy Storage Emerging: A Perspective from the Joint Center for Energy Storage Research. *Proc. Natl. Acad. Sci. U. S. A.* **2020**, *117* (23), 12550–12557.

(16) Dunn, B.; Kamath, H.; Tarascon, J.-M. Electrical Energy Storage for the Grid: A Battery of Choices. *Science (80-.).* **2011**, *334* (6058), 928–935.

(17) Alotto, P.; Guarnieri, M.; Moro, F. Redox Flow Batteries for the Storage of Renewable Energy: A Review. *Renew. Sustain. Energy Rev.* **2014**, *29*, 325–335.

(18) Ravikumar, M. K.; Rathod, S.; Jaiswal, N.; Patil, S.; Shukla, A. The Renaissance in Redox Flow Batteries. *J. Solid State Electrochem.* **2017**, *21* (9), 2467–2488.

(19) Sánchez-Díez, E.; Ventosa, E.; Guarnieri, M.; Trovò, A.; Flox, C.; Marcilla, R.; Soavi, F.; Mazur, P.; Aranzabe, E.; Ferret, R. Redox Flow Batteries: Status and Perspective towards Sustainable Stationary Energy Storage. *J. Power Sources* **2021**, *481*, 228804.

(20) Alotto, P.; Guarnieri, M.; Moro, F. Redox Flow Batteries for the Storage of Renewable Energy: A Review. *Renew. Sustain. Energy Rev.* **2014**, *29*, 325–335.

(21) Park, M.; Ryu, J.; Wang, W.; Cho, J. Material Design and Engineering of Next-Generation Flow-Battery Technologies. *Nat. Rev. Mater.* **2017**, *2*, 16080.

(22) Rhodes, Z.; Cabrera-Pardo, J. R.; Li, M.; Minteer, S. D. Electrochemical Advances in Non-Aqueous Redox Flow Batteries. *Isr. J. Chem.* **2021**, *61* (1–2), 101–112.

(23) Kortekaas, L.; Fricke, S.; Korshunov, A.; Cekic-Laskovic, I.; Winter, M.; Grünebaum, M. Building Bridges: Unifying Design and Development Aspects for Advancing Non-Aqueous Redox-Flow Batteries. *Batteries* **2022**, *9* (1), 4.

(24) Winsberg, J.; Hagemann, T.; Janoschka, T.; Hager, M. D.; Schubert, U. S. Redox-Flow Batteries: From Metals to Organic Redox-Active Materials. *Angew. Chemie - Int. Ed.* **2017**, *56* (3), 686–711.

(25) Kim, J.; Kim, Y.; Yoo, J.; Kwon, G.; Ko, Y.; Kang, K. Organic Batteries for a Greener Rechargeable World. *Nat. Rev. Mater.* **2022**, *8* (1), 54–70.

(26) Shrestha, A.; Hendriks, K. H.; Sigman, M. S.; Minteer, S. D.; Sanford, M. S. Realization of an Asymmetric Non-Aqueous Redox Flow Battery through Molecular Design to Minimize Active Species Crossover and Decomposition. *Chem. – A Eur. J.* **2020**, *26* (24), 5369–5373.

(27) Perry, M. L.; Saraidaridis, J. D.; Darling, R. M. Crossover Mitigation Strategies for Redox-Flow Batteries. *Curr. Opin. Electrochem.* **2020**, *21* (11), 311–318.

(28) Potash, R. A.; McKone, J. R.; Conte, S.; Abruña, H. D. On the Benefits of a Symmetric Redox Flow Battery. *J. Electrochem. Soc.* **2016**, *163* (3), A338–A344.

(29) Janoschka, T.; Friebe, C.; Hager, M. D.; Martin, N.; Schubert, U. S. An Approach Toward Replacing Vanadium: A Single Organic Molecule for the Anode and Cathode of an Aqueous Redox-Flow Battery. *ChemistryOpen* **2017**, *6* (2), 216–220.

(30) Lourenssen, K.; Williams, J.; Ahmadpour, F.; Clemmer, R.; Tasnim, S. Vanadium Redox

Flow Batteries: A Comprehensive Review. *J. Energy Storage* **2019**, *25* (June), 100844.

(31) Chen, R. Redox Flow Batteries: Mitigating Cross-Contamination via Bipolar Redox-Active Materials and Bipolar Membranes. *Curr. Opin. Electrochem.* **2023**, *37*, 101188.

(32) Li, M.; Case, J.; Minteer, S. D. Bipolar Redox-Active Molecules in Non-Aqueous Organic Redox Flow Batteries: Status and Challenges. *ChemElectroChem* **2021**, *8* (7), 1215–1232.

(33) Li, M.; Agarwal, G.; Shkrob, I. A.; VanderLinden, R. T.; Case, J.; Prater, M.; Rhodes, Z.; Assary, R. S.; Minteer, S. D. Critical Role of Structural Order in Bipolar Redox-Active Molecules for Organic Redox Flow Batteries. *J. Mater. Chem. A* **2021**, *9* (41), 23563–23573.

(34) Kosswattaarachchi, A. M.; Friedman, A. E.; Cook, T. R. Characterization of a BODIPY Dye as an Active Species for Redox Flow Batteries. *ChemSusChem* **2016**, *9* (23), 3317–3323.

(35) Ma, T.; Pan, Z.; Miao, L.; Chen, C.; Han, M.; Shang, Z.; Chen, J. Porphyrin-Based Symmetric Redox-Flow Batteries towards Cold-Climate Energy Storage. *Angew. Chemie* **2018**, *130* (12), 3212–3216.

(36) Geysens, P.; Li, Y.; Vankelecom, I.; Fransaer, J.; Binnemans, K. Highly Soluble 1,4-Diaminoanthraquinone Derivative for Nonaqueous Symmetric Redox Flow Batteries. *ACS Sustain. Chem. Eng.* **2020**, *8* (9), 3832–3843.

(37) Tracy, J. S.; Horst, E. S.; Roytman, V. A.; Toste, F. D. Development of High-Voltage Bipolar Redox-Active Organic Molecules through the Electronic Coupling of Catholyte and Anolyte Structures. *Chem. Sci.* **2022**, *13* (36), 10806–10814.

(38) Liu, Y.; Dai, G.; Chen, Y.; Wang, R.; Li, H.; Shi, X.; Zhang, X.; Xu, Y.; Zhao, Y. Effective Design Strategy of Small Bipolar Molecules through Fused Conjugation toward 2.5 V Based Redox Flow Batteries. *ACS Energy Lett.* **2022**, *7* (4), 1274–1283.

(39) Steen, J. S.; Nuismer, J. L.; Eiva, V.; Wiglema, A. E. T.; Daub, N.; Hjelm, J.; Otten, E. Blatter Radicals as Bipolar Materials for Symmetrical Redox-Flow Batteries. *J. Am. Chem. Soc.* **2022**, *144* (11), 5051–5058.

(40) Dmello, R.; Milshtein, J. D.; Brushett, F. R.; Smith, K. C. Cost-Driven Materials Selection Criteria for Redox Flow Battery Electrolytes. *J. Power Sources* **2016**, *330*, 261–272.

(41) Moutet, J.; El-Assaad, T. H.; Kaur, R.; Mills, D. D.; Gianetti, T. L. Designing the next Generation of Symmetrical Organic Redox Flow Batteries Using Helical Carbocations. *Energy Mater.* **2024**, *4* (3).

(42) Winsberg, J.; Stolze, C.; Muench, S.; Liedl, F.; Hager, M. D.; Schubert, U. S. TEMPO/Phenazine Combi-Molecule: A Redox-Active Material for Symmetric Aqueous Redox-Flow Batteries. *ACS Energy Lett.* **2016**, *1* (5), 976–980.

(43) Duan, W.; Vemuri, R. S.; Milshtein, J. D.; Laramie, S.; Dmello, R. D.; Huang, J.; Zhang, L.; Hu, D.; Vijayakumar, M.; Wang, W.; Liu, J.; Darling, R. M.; Thompson, L.; Smith, K.; Moore, J. S.; Brushett, F. R.; Wei, X. A Symmetric Organic-Based Nonaqueous Redox Flow Battery and Its State of Charge Diagnostics by FTIR. *J. Mater. Chem. A*

2016, *4* (15), 5448–5456.

(44) Moutet, J.; Veleta, J. M.; Gianetti, T. L. Symmetric, Robust, and High-Voltage Organic Redox Flow Battery Model Based on a Helical Carbenium Ion Electrolyte. *ACS Appl. Energy Mater.* **2021**, *4* (1), 9–14.

(45) Moutet, J.; Mills, D.; Hossain, M. M.; Gianetti, T. L. Increased Performance of an All-Organic Redox Flow Battery Model via Nitration of the [4]Helicenium DMQA Ion Electrolyte. *Mater. Adv.* **2022**, *3* (1), 216–223.

(46) Moutet, J.; Mills, D. D.; Lozier, D. L.; Gianetti, T. L. [4]Helicenium Ion as Bipolar Redox Material for Symmetrical Fully Organic Pole-less Redox Flow Battery. *Batter. Supercaps* **2024**, *7* (4), 1–33.

(47) Moutet, J.; Nowack, M. H.; Mills, D. D.; Lozier, D. L.; Laursen, B. W.; Gianetti, T. L. Planar Carbenium Ions for Robust Symmetrical All Organic Redox Flow Batteries. *Mater. Adv.* **2023**, *4* (19), 4598–4606.

(48) Mei, L.; Veleta, J. M.; Gianetti, T. L. Helical Carbenium Ion: A Versatile Organic Photoredox Catalyst for Red-Light-Mediated Reactions. *J. Am. Chem. Soc.* **2020**, *142* (28), 12056–12061.

(49) Mei, L.; Gianetti, T. Helical Carbenium Ion-Based Organic Photoredox Catalyst: A Versatile and Sustainable Option in Red-Light-Induced Reactions. *Synlett* **2020**, *31*, A-G.

(50) Nowack, M. H.; Moutet, J.; Laursen, B. W.; Gianetti, T. L. Triangulenium Ions: Versatile Organic Photoredox Catalysts for Green-Light-Mediated Reactions. *Synlett* **2023**, *35* (03), 307–312.

(51) Romero, N. A.; Nicewicz, D. A. Organic Photoredox Catalysis. *Chem. Rev.* **2016**, *116* (17), 10075–10166.

(52) Vega-Peñaloza, A.; Mateos, J.; Companyó, X.; Escudero-Casao, M.; Dell'Amico, L. A Rational Approach to Organo-Photocatalysis: Novel Designs and Structure-Property Relationships. *Angew. Chemie Int. Ed.* **2021**, *60* (3), 1082–1097.

(53) Hossain, M. M.; Shaikh, A. C.; Moutet, J.; Gianetti, T. L. Photocatalytic α-Arylation of Cyclic Ketones. *Nat. Synth.* **2022**, *1* (2), 147–157.

(54) White, A.; Wang, L.; Nicewicz, D. Synthesis and Characterization of Acridinium Dyes for Photoredox Catalysis. *Synlett* **2019**, *30* (07), 827–832.

(55) Laursen, B. W.; Krebs, F. C. Synthesis of a Triazatriangulenium Salt. *Angew. Chemie* **2000**, *39* (19), 3432–3434.

(56) Laleu, B.; Herse, C.; Laursen, B. W.; Bernardinelli, G.; Lacour, J. Bent Structure and Dynamic Stereochemistry of Chiral Acridinium Cations. *J. Org. Chem.* **2003**, *68* (16), 6304–6308.

(57) Nicolas, C.; Herse, C.; Lacour, J. Catalytic Aerobic Photooxidation of Primary Benzylic Amines Using Hindered Acridinium Salts. *Tetrahedron Lett.* **2005**, *46* (27), 4605–4608.

(58) Wilger, D. J.; Gesmundo, N. J.; Nicewicz, D. A. Catalytic Hydrotrifluoromethylation of

Styrenes and Unactivated Aliphatic Alkenes via an Organic Photoredox System. *Chem. Sci.* **2013**, *4* (8), 3160.

(59) Fukuzumi, S.; Kotani, H.; Ohkubo, K.; Ogo, S.; Tkachenko, N. V.; Lemmetyinen, H. Electron-Transfer State of 9-Mesityl-10-Methylacridinium Ion with a Much Longer Lifetime and Higher Energy Than That of the Natural Photosynthetic Reaction Center. *J. Am. Chem. Soc.* **2004**, *126* (6), 1600–1601.

(60) Kotani, H.; Ohkubo, K.; Fukuzumi, S. Photocatalytic Oxygenation of Anthracenes and Olefins with Dioxygen via Selective Radical Coupling Using 9-Mesityl-10-Methylacridinium Ion as an Effective Electron-Transfer Photocatalyst. *J. Am. Chem. Soc.* **2004**, *126* (49), 15999–16006.

(61) Romero, N. A.; Margrey, K. A.; Tay, N. E.; Nicewicz, D. A. Site-Selective Arene C-H Amination via Photoredox Catalysis. *Science (80-.).* **2015**, *349* (6254), 1326–1330.

(62) Joshi-Pangu, A.; Lévesque, F.; Roth, H. G.; Oliver, S. F.; Campeau, L. C.; Nicewicz, D.; DiRocco, D. A. Acridinium-Based Photocatalysts: A Sustainable Option in Photoredox Catalysis. *J. Org. Chem.* **2016**, *81* (16), 7244–7249.

(63) Wang, H.; Sayed, S. Y.; Luber, E. J.; Olsen, B. C.; Shirurkar, S. M.; Venkatakrishnan, S.; Tefashe, U. M.; Farquhar, A. K.; Smotkin, E. S.; McCreery, R. L.; Buriak, J. M. Redox Flow Batteries: How to Determine Electrochemical Kinetic Parameters. *ACS Nano* **2020**, *14* (3), 2575–2584.

(64) Nicholson, R. S. Theory and Application of Cyclic Voltammetry for Measurement of Electrode Reaction Kinetics. *Anal. Chem.* **1965**, *37* (11), 1351–1355.

(65) Lavagnini, I.; Antiochia, R.; Magno, F. An Extended Method for the Practical Evaluation of the Standard Rate Constant from Cyclic Voltammetric Data. *Electroanalysis* **2004**, *16* (6), 505–506.

(66) Greco, K. V; Forner-Cuenca, A.; Mularczyk, A.; Eller, J.; Brushett, F. R. Elucidating the Nuanced Effects of Thermal Pretreatment on Carbon Paper Electrodes for Vanadium Redox Flow Batteries. *ACS Appl. Mater. Interfaces* **2018**, *10* (51), 44430–44442.

(67) Milshtein, J. D.; Barton, J. L.; Carney, T. J.; Kowalski, J. A.; Darling, R. M.; Brushett, F. R. Towards Low Resistance Nonaqueous Redox Flow Batteries. *J. Electrochem. Soc.* **2017**, *164* (12), A2487–A2499.